frontiers | Frontiers in Earth Science

TYPE Original Research
PUBLISHED 19 February 2025
DOI 10.3389/feart.2025.1551716

OPEN ACCESS

EDITED BY
Hong-Hu Zhu,
Nanjing University, China

REVIEWED BY
Lei Zhang,
China University of Geosciences, China
Xiao Ye,
Nanjing University of Information Science and Technology, China

*CORRESPONDENCE
Chunmei Zhou,
2564937223@qq.com

RECEIVED 26 December 2024
ACCEPTED 30 January 2025
PUBLISHED 19 February 2025

CITATION
Li G, Zhou C, Qin Z and Xing H (2025) Study on the soil arching effect and evolution mechanism of anti-sliding pile in accumulation layers landslides under reservoir water level fluctuations.
Front. Earth Sci. 13:1551716.
doi: 10.3389/feart.2025.1551716

Study on the soil arching effect and evolution mechanism of anti-sliding pile in accumulation layers landslides under reservoir water level fluctuations

Guangbo Li, Chunmei Zhou*, Zihan Qin and Haiguang Xing

School of Civil Engineering and Architecture, Wuhan Institute of Technology, Wuhan, China

This study focuses on the Shilongmen landslide in the Three Gorges Reservoir area, investigating the evolution of the soil arching effect and its influencing factors in the context of landslide disaster prevention and control. Through field investigation, theoretical analysis, and FLAC3D numerical simulations, the effects of factors such as reduced soil strength parameters, and soil slip in front of piles on the soil arching effect were systematically analyzed. The numerical simulations specifically examined the stress distribution of the soil arching effect along the depth direction and its stages of evolution during the landslide process. The results indicate that when soil strength parameters are low, stress variations along the soil depth increase. As strength parameters continue to decrease, the load-bearing capacity of the soil arching effect weakens, resulting in increased internal stress within the landslide body. Soil slip in front of the piles significantly reduces the frictional soil arching effect, with stress in the surface soil decreasing by approximately 50%. The study identified three stages of the soil arching effect: initiation, development, and failure. Under the combined influence of multiple factors, the friction soil arch slides along the sides of the anti-slide piles, while the bearing capacity of the soil at the end-bearing soil arch is approximately 1.5 times higher than that of the friction soil arch. Due to deformation incompatibility between anti-slide piles and the surrounding soil, pile-soil separation may occur, suggesting that anti-slide pile designs should incorporate baffle structures to enhance overall stability. These findings provide a novel perspective and approach for optimizing anti-slide pile design and landslide disaster prevention, contributing to improved safety and reliability in landslide mitigation engineering.

KEYWORDS

three gorges reservoir area, landslide, anti-slide piles, soil arching effects, FLAC 3D

1 Introduction

The soil arching effect between anti-slide piles and the soil plays a crucial role in the design and analysis of anti-slide piles. This phenomenon reflects the arch-shaped stress distribution pattern around the piles, significantly influencing the bearing capacity and stability of the piles. Researchers have explored various aspects of landslides and

the soil arching effect through theoretical analysis (Li et al., 2020; Chen et al., 2020), numerical simulation (Liu et al., 2020), and physical model experiments (Peeruna et al., 2020; Wang et al., 2024). Research on landslide mechanisms has primarily focused on the sources of landslide dynamics, incubation patterns, evolutionary stages, and states (Tang et al., 2022; Wang et al., 2023; Yu et al., 2022). Centrifugal modeling, as a typical physical simulation method, can be used to study the deformation and failure characteristics of landslides under various influencing factors (Fang et al., 2023). By combining field investigation, geological analysis, and advanced algorithms, the evolution characteristics of stepped sliding surfaces in landslides within the Three Gorges Reservoir area were thoroughly studied, and a new model for predicting landslide displacement was proposed (Li et al., 2021). Factors influencing pile-soil stability include hydrological changes, soil parameters, pile stiffness, and pile spacing (Fu, 2017; Hu et al., 2019; Xiang, 2019; Zhang et al., 2023). In the study of the soil arching effect, by analyzing the formation mechanism of the soil arching effect between anti-slide piles and incorporating the mechanical characteristics observed in actual engineering, a thrust calculation formula for the design of anti-slide piles considering the soil arching effect was derived to optimize the thrust calculation model (Liu et al., 2022). In terms of model tests, the anti-slide pile and soil model experiments revealed the failure mechanism of the soil arch during the sliding process and its uneven deformation characteristics (Zhong et al., 2022a; Zhong et al., 2022b). Through transparent soil model experiments, the effect of compaction on the soil arching effect was studied from the perspective of displacement changes, providing new research perspectives and insights (Ye et al., 2022).

Numerical simulation analysis has focused on establishing mechanical models through simulation software to explore conditions for arch formation, the principle of pile-soil interaction, and changing soil arch shapes (Liu et al., 2021; Ren et al., 2022). For example, using the fluid-solid coupling method, the FLAC 3D software was employed to study the pile-soil model under reservoir water level fluctuations and rainfall conditions. The results indicate that the landslide seepage field exhibits a dynamic response to water level fluctuations (Zhang, 2018). The strength reduction method was used for slope reliability analysis, and the optimal position for reinforcing slopes with anti-slide piles at the same pile spacing was proposed (Huang et al., 2020). The force behavior of stabilizing piles was simulated using PLAXIS 2D, and the impact of various environmental conditions, such as rainfall and reservoir water level fluctuations, on the performance of the stabilizing piles was analyzed (Zhou et al., 2014; Zhou et al., 2018). From the perspective of a true three-dimensional model, the soil arching effect of anti-slide piles and its impact on overall stability were studied (Xu, 2020). In addition, numerical simulation can be used to study the performance and stability of new drainage anti-slide piles, providing a new technical solution for landslide control (Li and Huang, 2023). Most existing studies focus on idealized conditions, often assuming that the soil in front of anti-slide piles remains stable and does not experience slippage. However, in actual engineering projects, external loads and rainfall frequently trigger soil movement in front of the piles, significantly influencing the soil arching effect. Soil slippage alters the geometry and size of the soil arch, which directly affects the bearing capacity of the piles. Despite the critical importance of this issue in engineering practice, it has received limited attention in previous research.

This study integrates numerical simulation and field investigation, using the Shilongmen accumulation layer landslide in the Three Gorges Reservoir area as the research subject to explore the evolution of the soil arching effect under the condition of soil slip in front of anti-slide piles. By analyzing stress and displacement contour maps from the numerical simulations of monitoring points, the study investigates the effects of soil slip and the weakening of soil parameters on the evolution of end-bearing and friction soil arches. Finally, the numerical simulation results are compared with field displacement monitoring data to validate the accuracy of the simulation, and further analysis is conducted on the influence of the slip process on the soil arching effect of anti-slide piles.

2 Landslide background

2.1 Shilongmen landslide

Figure 1 illustrates the geological and engineering overview of the Shilongmen Landslide in the Three Gorges Reservoir area, with the deformation area outlined in red. The site is reinforced with anti-slide piles, and monitoring points, exploration boreholes, and groundwater levels are marked for comprehensive analysis. This landslide, originating from the instability of Quaternary and recent loose accumulation layers, is classified as a colluvial landslide. The surrounding geological features include a variety of earth and rock formations, such as artificial fill, alluvial deposits, slope debris, talus, residual soil, and landslide accumulation. Figure 2 illustrates the geological profile along section AA' of the Shilongmen landslide, which extends approximately 175 m in length, with elevations ranging from 138 to 189 m. The geological composition in the Dazhou Town area consists of the New Quaternary system, the Suining Formation from the Upper Jurassic, and the Shaximiao Formation from the Middle Jurassic, progressing from northwest to southeast. The strata exhibit a monoclinic structure, with a dip direction of 299° and an apparent dip angle ranging from 5° to 30°. The landslide is located within the reservoir water fluctuation zone, particularly within the critical elevation range of 145–175 m. The area receives an average annual precipitation of 1,342.2 mm, mainly concentrated between May and September, with rainfall being a primary trigger for landslide activity. The landslide body has a thickness that varies from 8 to 20 m, averaging approximately 16 m. The rear edge of the landslide is characterized by a steep gradient, while the middle section has a more moderate slope.

2.2 Deformation characteristics of the Shilongmen landslide

According to the field investigation and geological exploration report, the whole part of the Shilongmen landslide is stable with some slow-moving local instabilities and an overall retrogressive style (Zeng et al., 2023). As shown in Figure 3, relative displacement monitoring data from four points within the Shilongmen landslide area reveal the actual displacement trends. Analysis from 2019 to 2020 indicates that the upper soil layers experienced greater

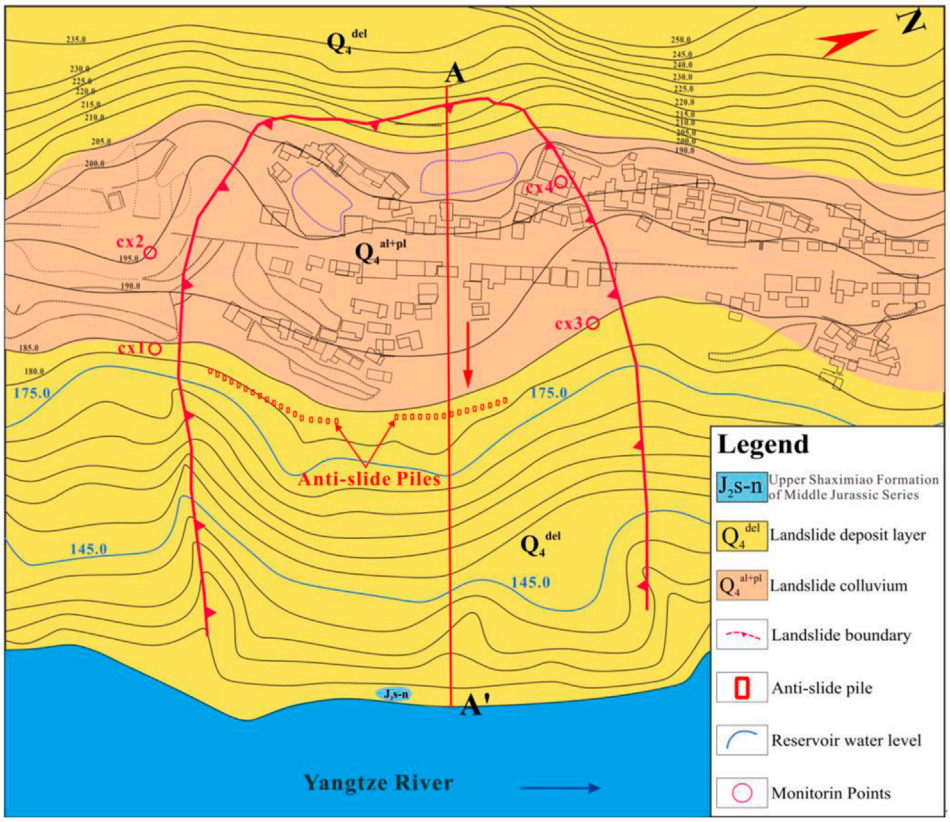

FIGURE 1
Shilongmen landslide in the Three Gorges reservoir area.

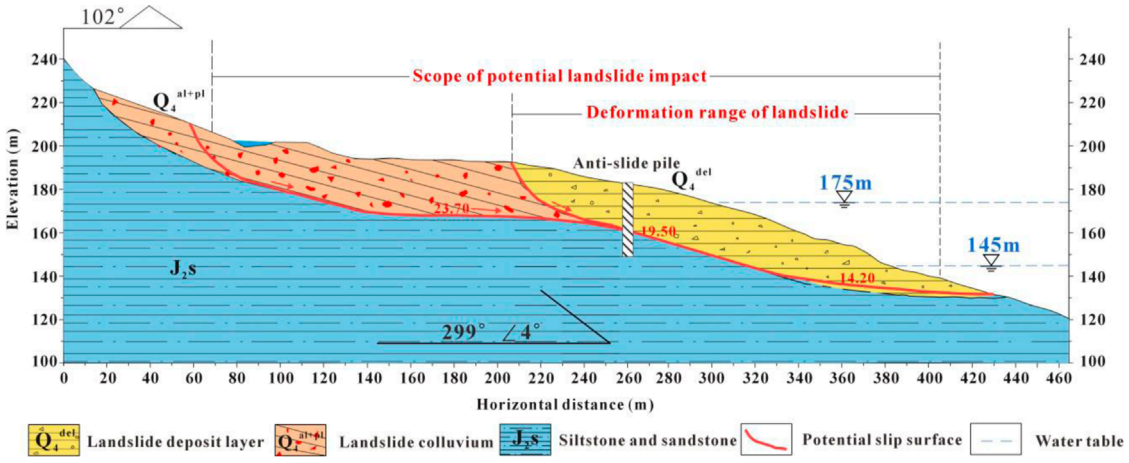

FIGURE 2
Geological profile along section AA′ of the Shilongmen landslide.

displacement compared to the lower layers. The most substantial displacement, recorded on 27 July 2020, reached approximately 40 mm at monitoring point three. Figure 3, which illustrates water level fluctuations in the Three Gorges Reservoir, shows that periods of significant displacement coincide with rapid changes in water levels. The displacement increase often occurs in the later stage of the reservoir water level decline (Xu et al., 2024). Over time, the magnitude of displacement gradually increased, with the primary displacement zone concentrated within the top 2–5 m of the surface, indicating the prevalence of shallow landslides in this area. The overall trend shows that displacement deformation decreases with depth, suggesting greater stability in deeper soil layers, which are less

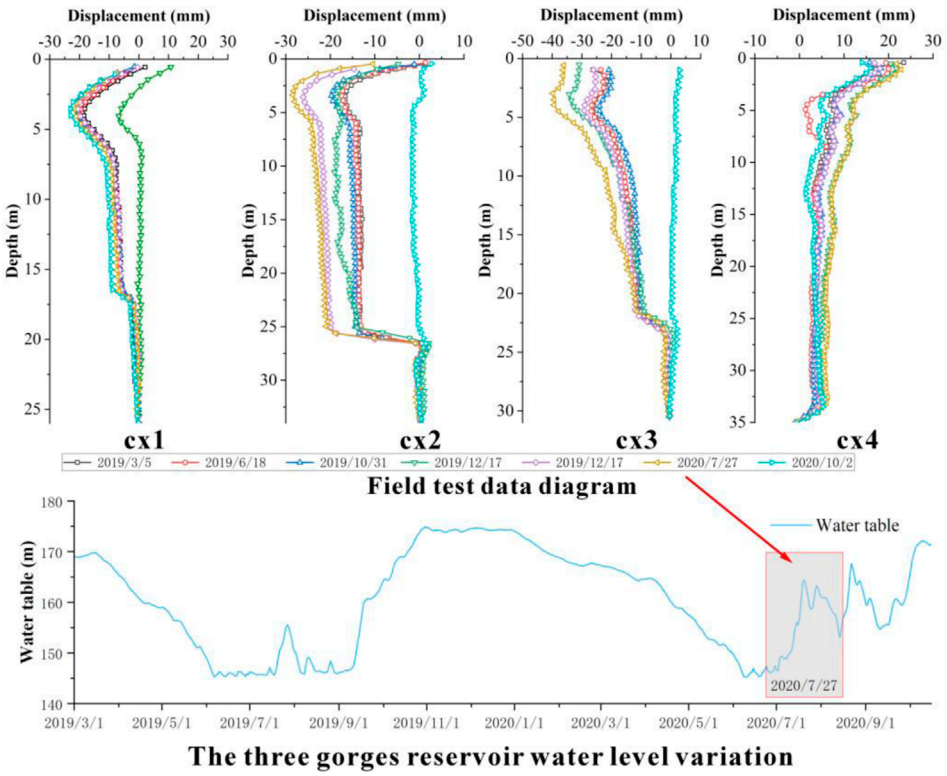

FIGURE 3
2019–2020 displacement monitoring data chart.

affected by surface displacement. Monitoring displacement is crucial for understanding the dynamic processes occurring within the Shilongmen landslide and for predicting future landslide behavior. This data provides essential support for landslide prevention and control efforts in geotechnical engineering, contributing to risk mitigation in similar regions.

The Shilongmen landslide was mitigated using anti-slide piles, which faced several challenges due to factors such as reservoir water level fluctuations. The original support structures sustained varying degrees of damage as a result. As shown in Figure 4A, significant slippage of the soil in front of the piles occurred over time, leading to the collapse of the soil between the piles. Notably, trees within the pile area also slipped along with the soil in front of the piles. The slippage of soil both in front of and between the anti-slide piles exposed the upper portions of the piles, causing them to appear in a near-cantilever state. Additionally, fractures were observed in the lock beams at the top of the anti-slide piles. Figure 4B presents a schematic of the geological conditions surrounding the anti-slide piles in reservoir bank landslides. Under the influence of external factors such as rainfall and reservoir water level fluctuations, the soil gradually slipped, resulting in uncoordinated deformation between the piles and the surrounding soil (Zhang et al., 2024). The forward sliding of the soil in front of the piles reduced its ability to bear the horizontal sliding force exerted on the upper sections of the piles. As a result, the lock beams in the anti-slide pile structure experienced increased shear forces, leading to cracking or deformation of the beams. Furthermore, as external loads persisted, the bearing capacity of the soil surrounding the piles gradually diminished. Ultimately, the soil between the piles, supported by a frictional soil arch, reached its bearing capacity, leading to a gradual collapse as the soil in front of the piles continued to slip.

3 Analysis of pile and soil force transfer principle

3.1 Analysis of soil arch evolution process

The interaction between anti-slide piles and the surrounding soil is notably complex, particularly under varying hydrological conditions, which significantly influence the stability and performance of the piles. Figure 5 illustrates the mechanical behavior of anti-slide piles under landslide conditions. In a stable state (Figure 5A), the soil in front of the pile remains unaffected by slippage or peeling. At this stage, the sliding force generated by the landslide is distributed between the anti-slide pile and the surrounding soil. The soil in front of the pile contributes to resisting the sliding force, and both the pile and the surrounding soil experience minimal displacement, maintaining overall stability. However, over time, periodic fluctuations in reservoir water levels induce forward sliding of the landslide soil in the cut-off zone ahead of the pile, as shown in Figure 5B. During this phase, rising water levels increase hydrostatic pressure, amplifying the sliding force of the landslide. Simultaneously, as the soil in front of the pile partially slips, its ability to resist sliding gradually weakens, resulting in a greater share of the landslide force being borne by the anti-slide

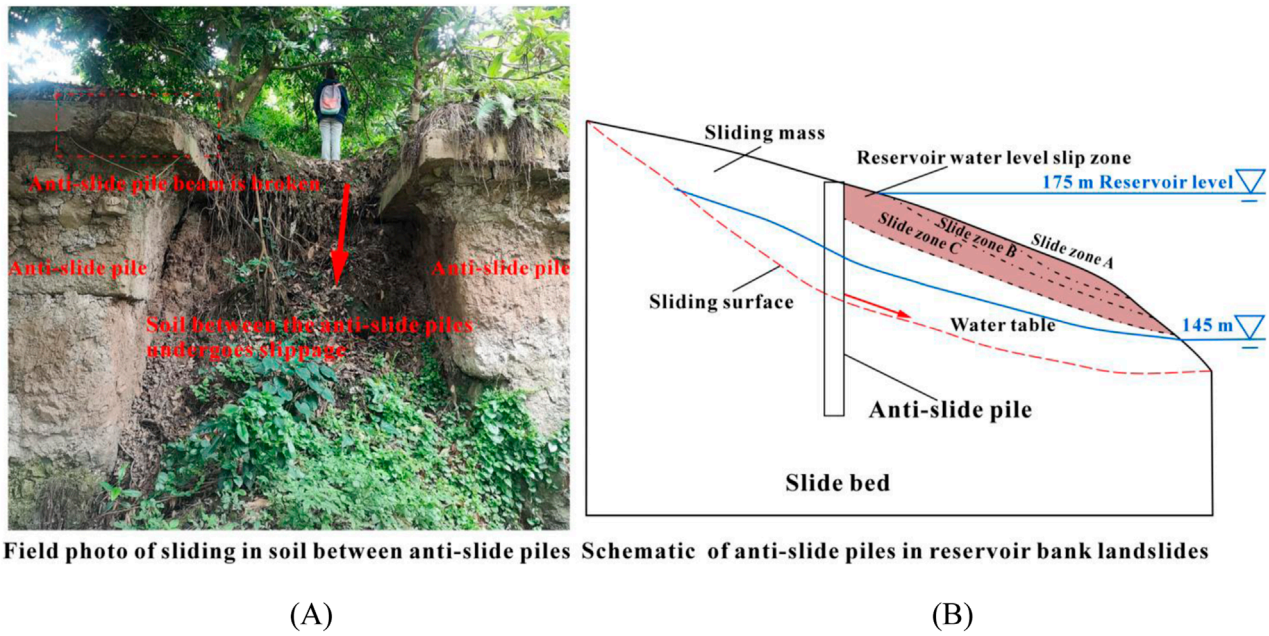

FIGURE 4
Diagram of deformation in anti-slide pile and surrounding soil **(A)** field photo of sliding in soil between anti-slide piles, **(B)** Schematic of anti-slide piles in reservoir bank landslides.

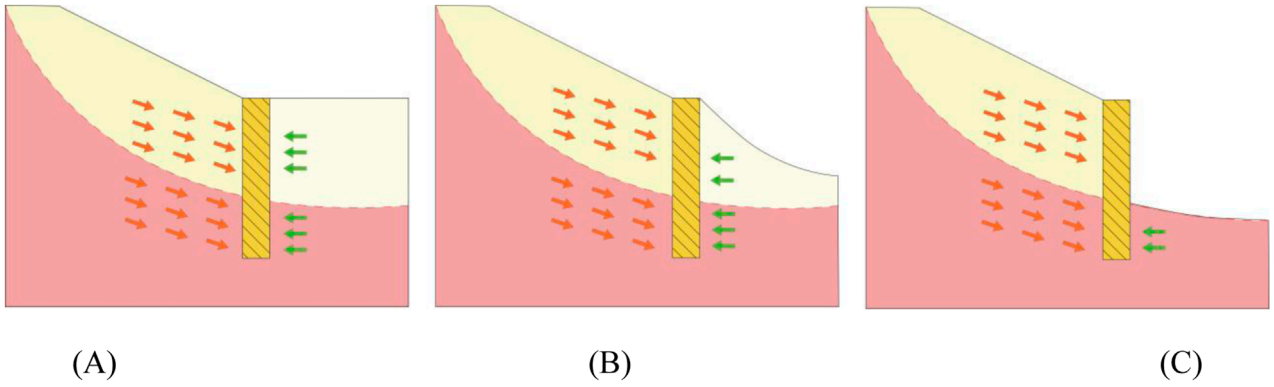

FIGURE 5
Mechanical analysis diagram of landslide anti-slide pile **(A)** Stable state, **(B)** Sliding state, **(C)** Slip completion state.

piles. As depicted in Figure 5C, by this stage, most of the soil in front of the pile has fully slipped, rendering it ineffective in resisting the landslide. The entire sliding force is then borne solely by the anti-slide piles, jeopardizing their stability. Regular fluctuations in water levels not only affect soil saturation and pore water pressure but can also alter the physical properties of the soil. These combined factors can lead to a reduction in the soil's strength around the piles, thereby diminishing the overall stability of the pile-soil system. Therefore, it is crucial to account for hydro-mechanical interactions and their implications for landslide dynamics when designing and evaluating anti-slide piles to ensure the long-term safety and stability of the structure.

The evolution of the soil arching effect can be divided into three distinct stages: the initial stage, the development stage, and the failure stage. As depicted in Figure 6, this process illustrates the progression of the soil arching effect. The red area represents the end-bearing soil arch, located primarily behind the anti-slide piles, which directly transmits the sliding force of the landslide to the piles. The green area between the piles represents the frictional soil arch. In the initial stage, the soil arching effect begins to form, with the frictional soil arch mainly concentrated on the rear side of the pile. At this point, the boundary between the end-bearing soil arch and the frictional soil arch is not well-defined. As adverse conditions persist, the soil arch develops along the sides of the piles, and the distinction between the end-bearing and frictional soil arches becomes more pronounced. During this stage, the soil arching effect lasts the longest. In the development stage, differing forces act on the end-bearing soil arch and the frictional soil arch,

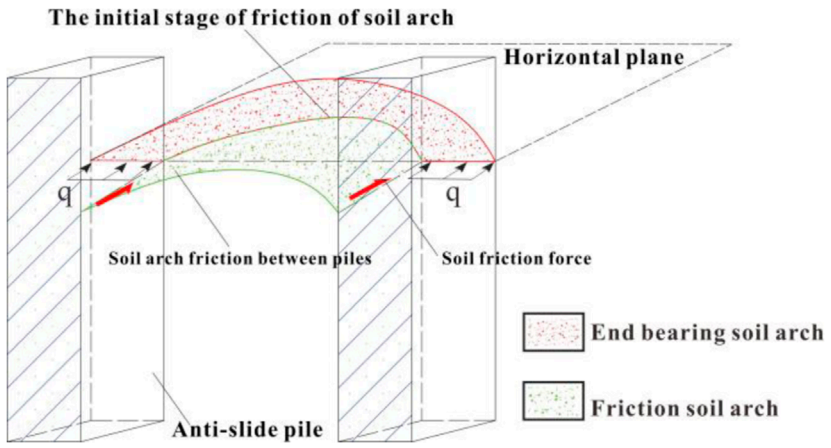

FIGURE 6
Diagram of the evolution of the soil arching effect.

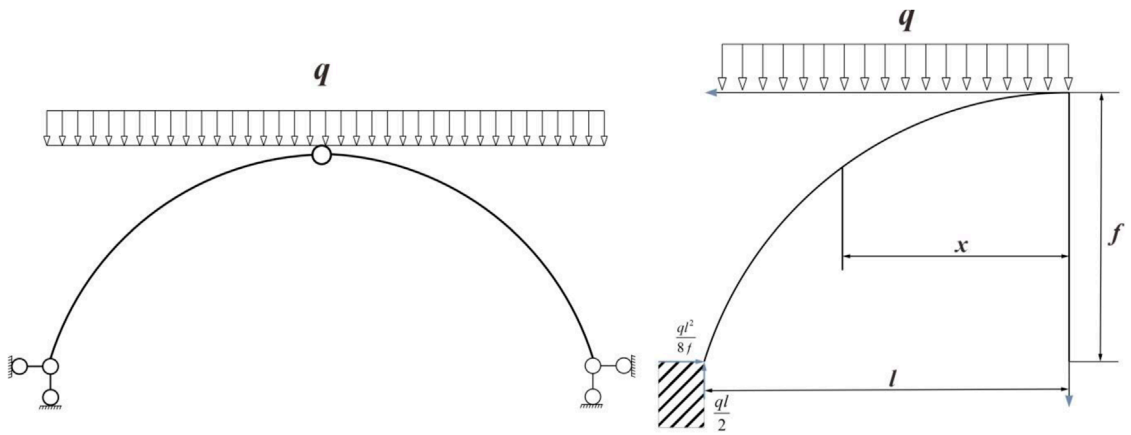

FIGURE 7
Arch force analysis diagram.

leading to stress differentials in the soil. This uneven distribution of stress causes surface cracks to appear. In the failure stage, as the soil in front of the pile begins to slide, the frictional soil arch continues to move along the sides of the pile until the soil reaches its maximum bearing capacity. Once the frictional soil arch can no longer transfer force to the sides of the anti-slide pile, this indicates the failure of the frictional soil arch. This failure results in a redistribution of stress within the soil and the collapse of the soil arch between the piles.

3.2 Two-dimensional soil arch plane mechanics analysis

Terzaghi (1943) expanded upon "The Granary Effect," originally observed in granular materials, to demonstrate its presence in soil bodies through active door experiments. With advancements in numerical simulation technology, studies have revealed that the soil arching effect primarily occurs as soil particles interconnect via stress chains to transfer forces to anti-slide piles (Zhang et al., 2021). Assuming treating the soil arch as a three-hinged arch in structural mechanics on a two-dimensional plane, the rational arch axis equation under a uniformly distributed load q can be derived based on fundamental principles of structural mechanics:

$$y = \frac{4f}{l^2}x(l-x) \tag{1}$$

In the Formula 1 and f respectively represent the clear span of the soil arch (i.e., the clear distance between piles) and the rise; the x and y-axes are illustrated as shown in Figure 7.

Under a reasonably designed arch axis, any cross-section experiences no shear force but only a horizontal thrust of magnitude. The anti-slide piles mainly bear the downward force generated by the landslide and the force transmitted from the end-supported soil arch effect in the y-direction. These two forces collectively play a pivotal role in stabilizing the landslide process. In the case of frictional soil arches, the force in the y-direction is borne by the friction between

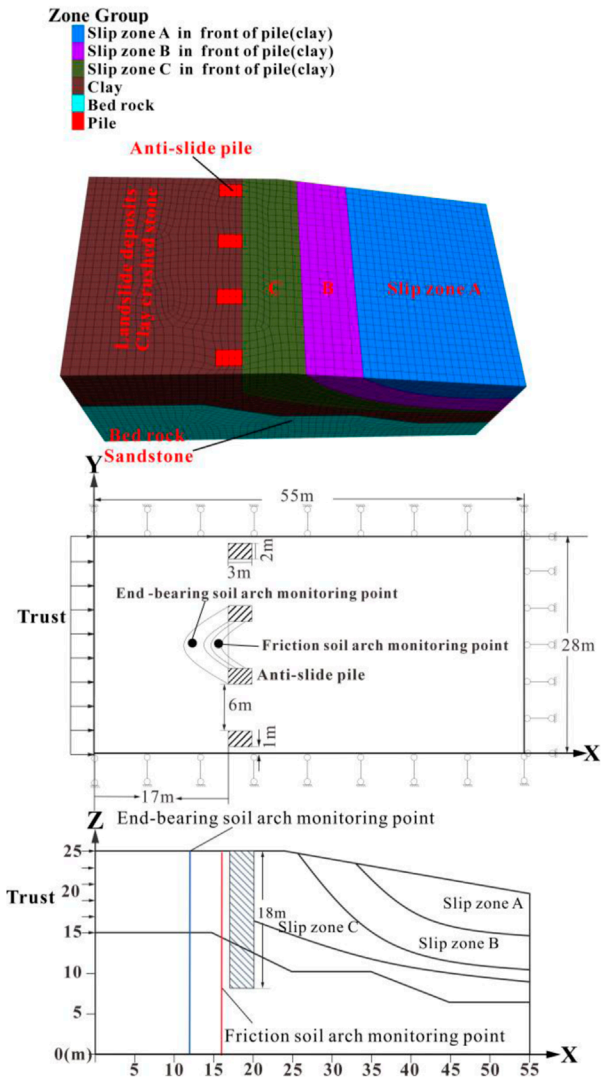

FIGURE 8
Model and monitoring site diagram.

TABLE 1 Numerical simulation parameters.

Name	P (kg/m^3)	E (pa)	c (kpa)	φ (°)	μ
Sliding Mass	2,100	5×10^7	20	20	0.3
Sandstone Layer	2,500	1.36×10^9	200	31	0.2
Pile	2,250	3×10^{10}	—	—	0.2

the soil and the anti-slide piles as well as the soil in front of the piles, rendering the bearing capacity of the frictional soil arch relatively weak. When the soil in front of the pile slips, the frictional soil arch between piles is more prone to damage and slips along with the soil in front of the piles. The investigation of q and l in the y-direction is crucial for the soil arch effect.

In landslide control engineering, stabilizing piles improve the overall shear strength of soil along potential sliding surfaces through

TABLE 2 Numerical simulation conditions.

Numerical simulation conditions	c (kpa)	φ(°)
	40	20
	30	20
Soil cohesion	20	20
	10	20
	5	20
	20	40
	20	30
Soil internal friction angle	20	20
	20	10
Pile front soil slippage	20	20

the soil arching effect, thereby achieving stability and balance within the soil mass. The shear strength of soil is typically expressed by the Mohr-Coulomb criterion:

$$\tau = c + \sigma \tan \phi \tag{2}$$

In the Formula 2, where τ represents the maximum shear stress the soil can withstand before failure, c is the cohesion, and ϕ is the internal friction angle. Higher cohesion and internal friction angles effectively increase the soil's resistance to sliding. When soil particles form an arch structure, the stabilizing forces generated counteract downslope and lateral displacements, effectively increasing the normal stress σ on the failure surface. The increased normal stress further enhances shear strength τ, thereby improving the overall stability of the soil mass. The soil arching effect transfers forces to the stabilizing piles, enabling the arch structure to bear greater shear stresses and allowing the soil mass to achieve equilibrium. In end-bearing soil arches, stabilizing piles provide strong vertical support to the arch structure, significantly increasing the stress σ on the failure surface and greatly enhancing the soil's shear resistance, which is crucial in maintaining stability. In contrast, frictional soil arches rely on weaker support, with stress transfer primarily dependent on friction between soil particles and the pile surface to maintain equilibrium. In both end-bearing and frictional soil arches, the soil arching effect contributes to stability by enhancing shear strength.

The stability of the soil arching effect is directly influenced by soil material properties, particularly cohesion and friction. Soils with high cohesion and friction favor the formation of stable soil arch structures, whereas soils with lower shear strength or loosely packed particles are more prone to arch failure, especially in frictional soil arches. This study will focus on numerically simulating the horizontal stress within the soil arching effect to explore its mechanisms in landslide control, providing quantitative parameters and practical guidance for engineering applications.

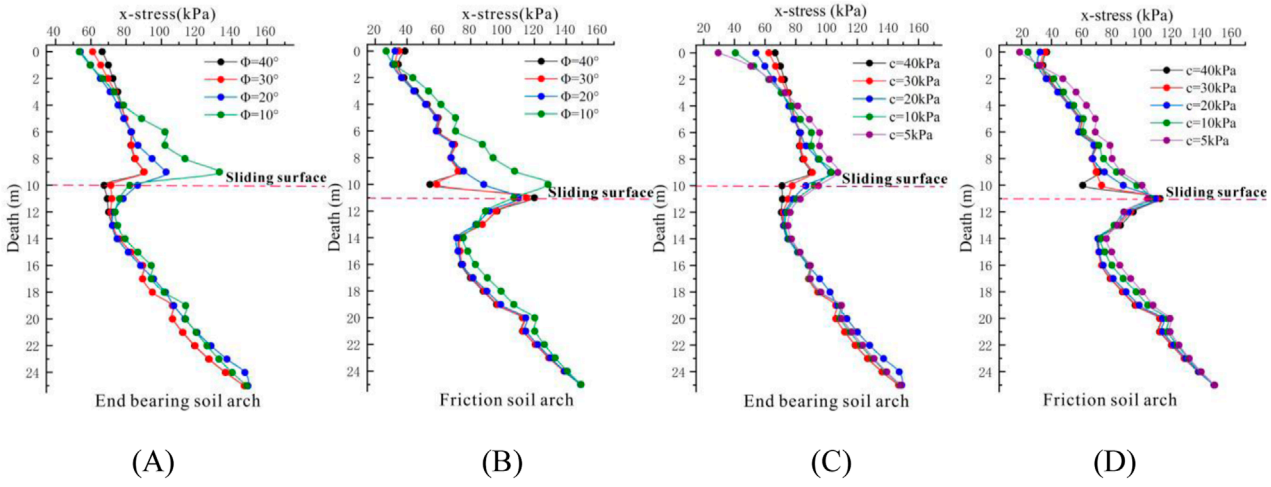

FIGURE 9
Xx stress diagram under varying shear strength parameter. **(A)** Effect of internal friction angle variation on end-bearing soil arch stress, **(B)** Effect of internal friction angle variation on frictional soil arch stress, **(C)** Effect of cohesion variation on end-bearing soil arch stress, **(D)** Effect of cohesion variation on frictional soil arch stress.

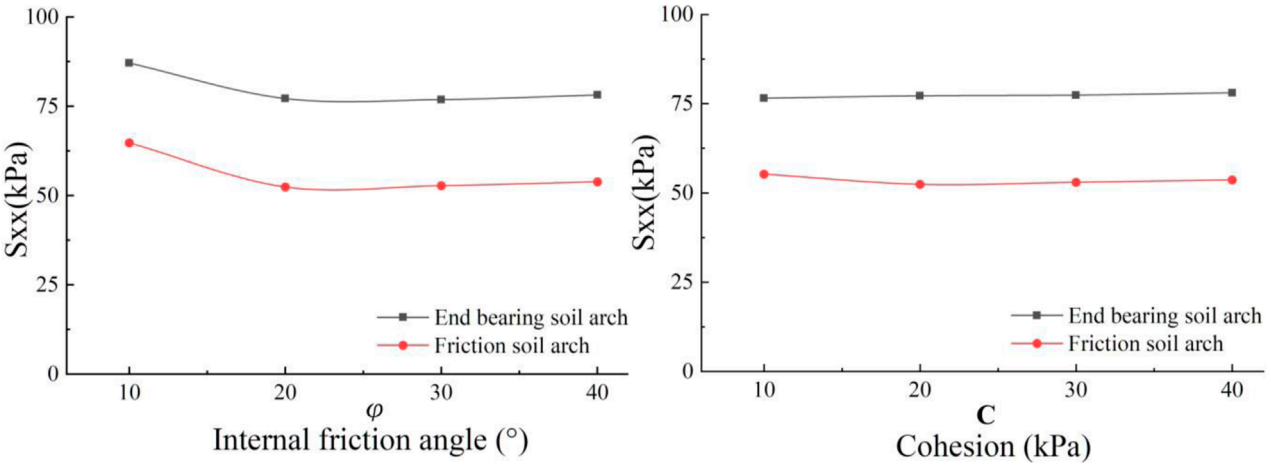

FIGURE 10
Xx average stress with different parameters.

4 Numerical simulation model and calculation results

4.1 Numerical simulation model

In this study, numerical simulations were conducted using FLAC3D, a widely used three-dimensional finite difference software in geotechnical engineering. The numerical model was initially created using Rhino software for 3D modeling, followed by mesh generation with Griddle 2.0, and the model was then imported into FLAC3D for analysis. The constructed model consists of 51,081 meshes and 42,376 nodes, providing a detailed representation of the model's structure and segmentation. The mechanical behavior of the soil and rock layers was simulated using the Mohr-Coulomb constitutive model, while the anti-slide piles were modeled with an elastic constitutive model. Additionally, slip zones were introduced in front of the anti-slide piles, labeled as Zone A, Zone B, and Zone C, to represent varying degrees of soil slippage.

Figure 8 illustrates the model dimensions and boundary conditions. The model is 55 m in length, 28 m in width, and has a height ranging from 15 to 25 m. The boundary conditions at the sides of the model are set as normal unidirectional constraints, while the bottommost rock layer is subjected to omnidirectional fixed constraints, and the landslide surface is treated as a free boundary. The anti-slide piles are designed with rectangular cross-sections, each 3 m long, 2 m wide, and a total length of 18 m. The spacing between the anti-slide piles is three times the width of the pile section, resulting in a center-to-center distance four times the width of the pile section. The piles are embedded into the rock layer to a depth of one-third of their total length, with an embedded end

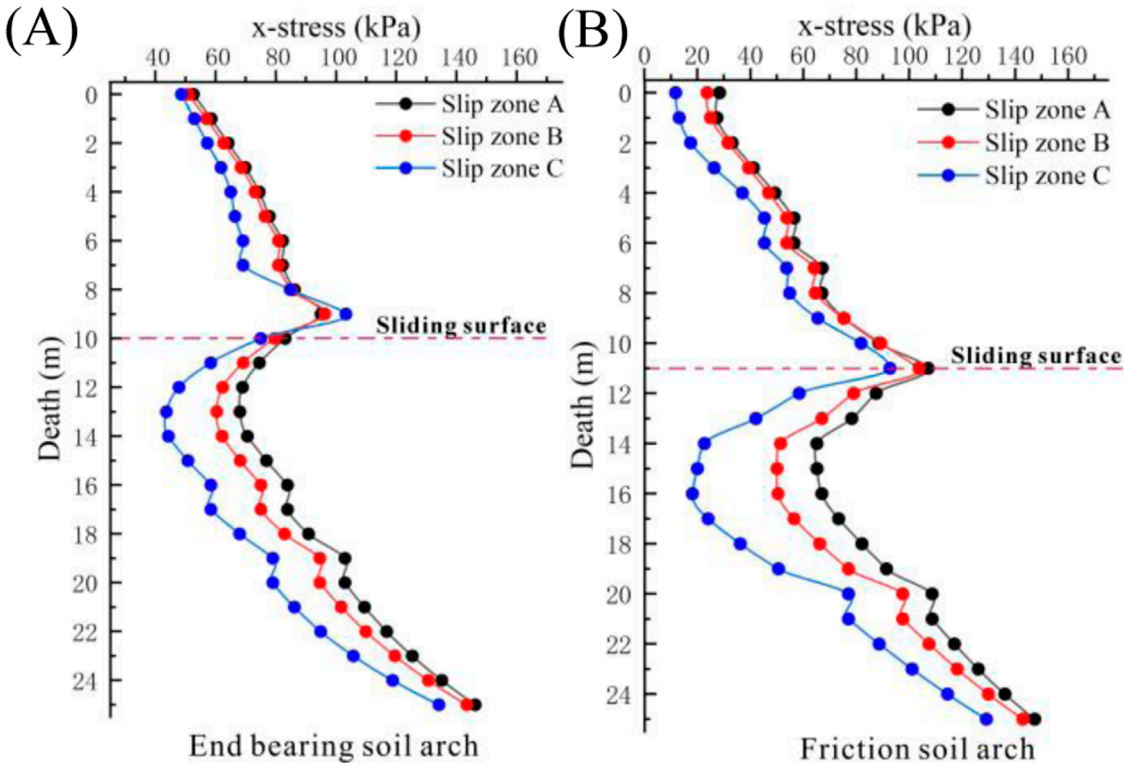

FIGURE 11
Xx stress diagram under varying slip zone. **(A)** Effect of slip zone variation on end-bearing soil arch stress, **(B)** Effect of slip zone variation on frictional soil arch stress.

length of 6 m. A horizontal stress load is applied to the clay layer, located 17 m away from the anti-slide piles. According to Figure 8, monitoring points A and B are used to observe the behaviors of the end-bearing and friction soil arches, respectively. Monitoring points are spaced 1 m apart along the depth of the soil body to analyze the distribution of the soil arching effect in the vertical direction. This model setup is intended to further investigate the mechanical responses of the soil-pile system under various conditions, with a particular focus on the influence of soil arching effects on the behavior of the anti-slide piles.

4.2 Numerical simulation conditions and parameters

In the study of landslide prevention and control in the Three Gorges Reservoir area, fluctuations in reservoir water levels play a crucial role in affecting landslide stability. These periodic changes cause the reservoir banks to undergo cycles of drying and wetting, leading to soil slippage, erosion, and subsequent alterations in soil strength parameters. As the number of dry-wet cycles increases, the strength parameters of the soil, such as cohesion and internal friction angle, degrade (Zhou et al., 2022). Consequently, varying values of cohesion and internal friction angle were used in the simulations to investigate how changes in these soil strength parameters influence the soil arching effect. In addition, the model simulates the impact of reservoir water level fluctuations on soil erosion by constructing different soil slip zones, and further reveals the complex interaction between the soil and anti-slide piles. The relevant working conditions and parameters for the numerical simulation are shown in Table 1, while the key parameters for the Shilongmen landslide numerical simulation are determined based on a comprehensive analysis of related numerical simulation results and physical experimental data (Zhu, 2022; Gao, 2023), as detailed in Table 2.

4.3 Calculation results of soil arch with different factors

4.3.1 The impact of changes in soil parameter on the soil arching effect

To investigate the effects of wet-dry cycling induced by repeated reservoir water level fluctuations on the soil arching effect, this study employs numerical simulations to analyze stress distribution patterns under various shear strength parameters. Figure 9A shows that, under different internal friction angles, the x-direction stress of the soil mass above the sliding surface increases gradually with depth and exhibits a sudden change near the sliding surface. The greatest abrupt stress variation occurs when the internal friction angle $\Phi = 10°$, while below the sliding surface, stress differences between internal friction angles are minimal. Similarly, within the frictional soil arch region, the soil exhibits a comparable trend, with the largest stress variation at the sliding surface observed for $\Phi =$

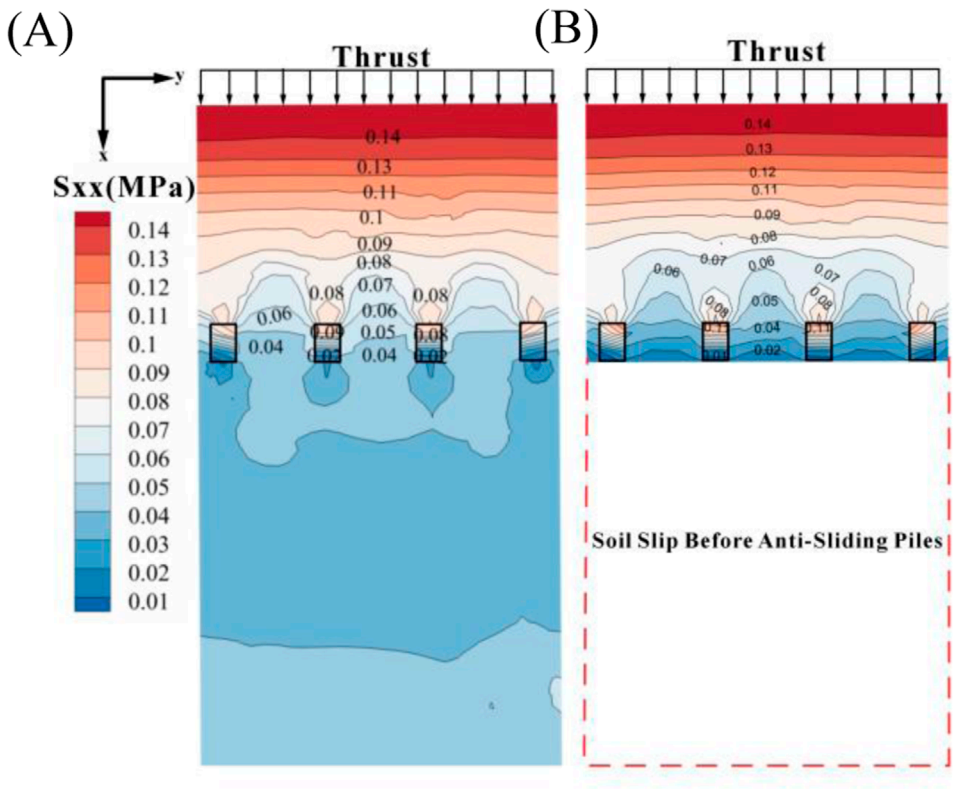

FIGURE 12
Stress nephogram under different working conditions. **(A)** Thrust only, **(B)** Soil slip in front of anti-slide piles.

10°, as illustrated in Figure 9B. Compared to end-bearing soil arches, frictional soil arches show a more rapid rate of stress variation along the depth under different internal friction angles. Insights from both figures indicate that a larger internal friction angle enhances the shear strength of the soil, thereby mitigating stress concentration near the sliding surface. Additionally, with larger internal friction angles, the stress level within the frictional soil arch region decreases. Furthermore, the stress values for internal friction angles of 30° and 40° are similar, suggesting that when the internal friction angle exceeds 30°, its impact on the soil arching effect tends to stabilize.

Figures 9C, D present the stress distribution in the end-bearing and frictional soil arch regions under varying cohesion levels. The figures show that as cohesion decreases from 40 kPa to 5 kPa, the variations in the stress distribution curve become more pronounced. At a cohesion level of 5 kPa, the stress change along the depth reaches its maximum; conversely, higher cohesion leads to a more uniform stress distribution, reducing stress concentration near the sliding surface. Figure 10 illustrates the average stress distribution of soil above sliding surfaces at various depths. With changes in cohesion and internal friction angle, the stress in the end-bearing soil arch region is approximately 1.5 times greater than that in the friction soil arch region. This demonstrates that the soil in the end-bearing soil arch region can support a higher load.

In summary, the analysis indicates that the force-transmission capacity of the end-bearing soil arch to the anti-slide piles is superior to that of the frictional soil arch. As the shear strength parameters of the soil decrease, the soil arching effect gradually weakens, leading to increasingly uneven stress transmission along the sliding surface, thereby heightening the risk of sliding. Additionally, the soil's ability to transfer force to the anti-slide piles decreases, while stress along the depth direction increases. With increases in both the internal friction angle and cohesion, the x-direction stress distribution curve becomes smoother, and the stress peak shifts closer to the sliding surface. This relationship suggests that high shear strength parameters not only inhibit sliding but also effectively balance stress distribution along the sliding surface, thereby reducing the risk of sudden sliding events.

4.3.2 The influence of soil slippage in front of the pile on the soil arch effect

Figure 11A illustrates the distribution of x-directional stress in the end-bearing soil arch in front of the piles under varying degrees of slip. From point A to point C, the slip range gradually increases, reaching its maximum in region C, where the anti-slide pile functions as a cantilever. Compared to the standard condition, the stress changes in the slip regions above the sliding surface (A and B) are relatively small; only upon reaching region C does the stress in the soil decrease. The underlying bedrock layer is also affected; as the slip area expands, the stress on the soil gradually diminishes. Figure 11B depicts the stress distribution of the friction soil arch under different slip regions. When the soil in front of the anti-slide pile slips into region C, the stress in the shallow soil above the sliding surface drops to 50% of that under standard conditions. At this point, the friction soil arch in the surface soil may

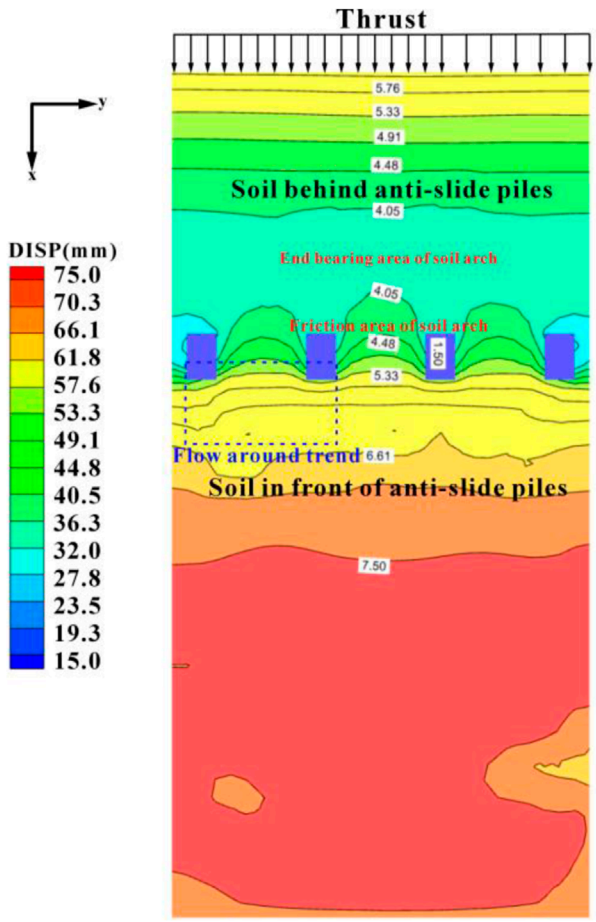

FIGURE 13
Displacement nephogram at 5 m depth under thrust.

experience structural failure, leading to a weakening of the friction effect and a corresponding reduction in the supporting capacity of the pile.

As the degree of slip increases (from slip regions A to C), the x-directional stress in the soil gradually decreases, particularly evident above and below the sliding surface. This may be attributed to stress release and redistribution caused by the slip, resulting in reduced horizontal stress on the soil above and below the sliding surface. There are significant differences in response between the end-bearing soil arch and the friction soil arch regarding slip; the friction soil arch is more sensitive to soil slip in front of the pile. To ensure the stability of the pile support structure, it is essential to accurately monitor and control the range and depth of soil slip, ensuring they remain within safe limits.

4.3.3 The influence of soil arch effect under multifactorial conditions

Figure 12A shows the x-direction stress contour of the soil mass in front of the pile when no slip occurs. In this scenario, the end-bearing soil arch and friction soil arch are closely connected, with fewer friction soil arches but higher arch heights. However, when external conditions cause the soil mass in front of the pile to slip, the configuration of the soil arches changes significantly, as shown in Figure 12B. The blank area indicates that the soil in front of the anti-slide piles at this depth has slipped, with the friction soil arches moving forward along both sides of the piles, and their number increasing noticeably. This change results in a significant increase in the horizontal stress within the soil and a reduction in the height of the friction soil arches. When the soil mass in front of the pile slips, the anti-slide capacity of the pile is weakened, leading to increased internal stress within the soil arch between the piles and a shift in the distribution of the soil arches. As the bearing capacity of the soil between the piles becomes insufficient, the frictional effect of the soil arch gradually weakens, causing a redistribution of stress in the soil, which eventually leads to the collapse of the soil mass between the piles and a loss of the supporting effectiveness of the anti-slide piles.

Figure 13 presents a displacement cloud diagram at a depth of 5 m under isolated thrust action, illustrating the displacement behavior of anti-slide piles subjected to an external thrust of 150 kPa. The diagram shows a notable concentration of displacement within the anti-slide piles, as indicated by the rectangular zone, where displacement values are relatively minimal. This phenomenon results from the material properties of the anti-slide piles, combined with the anchoring effect provided by the fixed end embedded in the rock layer, contributing to their sustained stability under external load. Within the scope of the soil arch effect triggered by the thrust, soil displacement is significantly lower compared to other regions, with the displacement of the soil between the piles slightly exceeding that in the end-bearing soil arch zone. This highlights the substantial influence of anti-slide piles on controlling soil displacement behind them. Discrepancies in displacement between the anti-slide piles and the surrounding soil are evident, with greater displacement observed in the soil ahead of the piles, reflecting the actual engineering scenario depicted in the figure. Such variations in displacement distribution could exacerbate the degradation and failure of anti-slide pile support structures, potentially affecting project stability. Additionally, in the blue-delineated region of the figure, both the anti-slide piles and the soil in front exhibit a tendency to flow and divert around the piles. To ensure project stability, careful consideration must be given to the deformation interaction between the piles and the surrounding soil.

Figure 14 presents the monitoring results of soil displacement under thrust, providing displacement data for both the end-bearing soil arch and the friction soil arch between the piles. The results show a consistent decrease in displacement with depth, aligning with the displacement distribution trends depicted in Figure 3 cx3. Notably, soil displacement at the inter-pile frictional soil arch differs significantly from that at the end-bearing soil arch, primarily due to uncoordinated soil deformation around the pile. The data underscore the importance of inter-pile retaining boards in managing soil displacement between piles in similar engineering projects.

5 Discussion

The soil arching effect is a pivotal factor in the stability of anti-slide piles, particularly in the context of reservoir bank

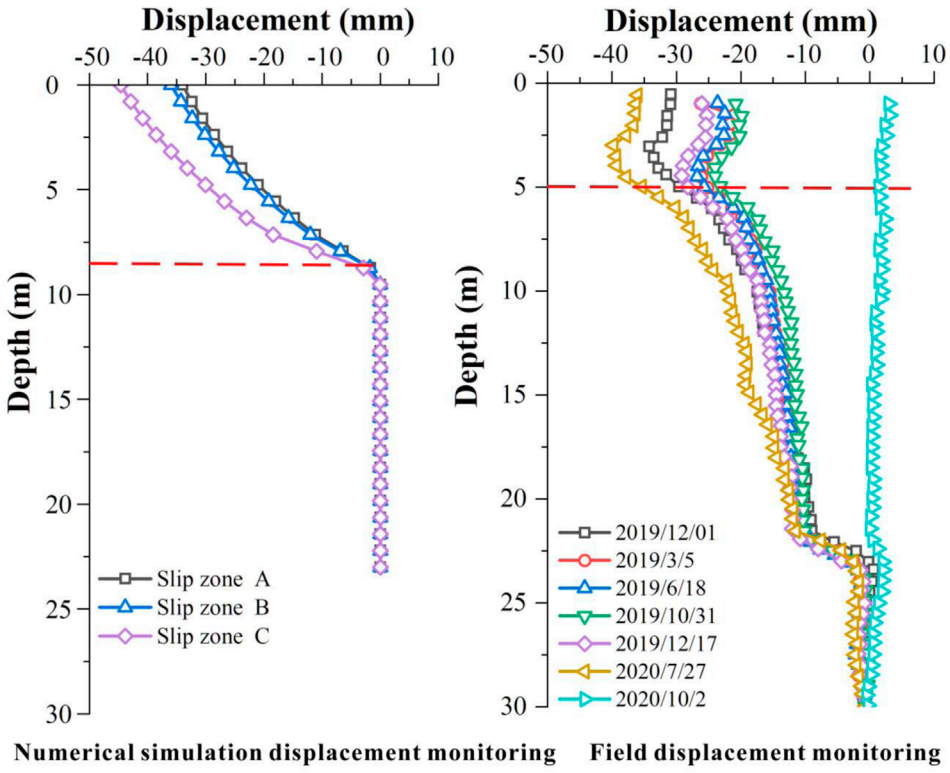

FIGURE 14
Displacement monitoring diagram under thrust action.

landslides, where its influence is pronounced. This effect is contingent upon the soil's shear strength parameters, such as the internal friction angle and cohesion, as well as external factors such as reservoir water level fluctuations. Studies have shown that as the internal friction angle diminishes, the soil's capacity for effective stress transmission decreases, leading to an increase in internal stress. Moreover, prolonged exposure to fluctuating water levels weakens soil cohesion, prompting stress redistribution and further reducing the soil arching effect. Soil slip in front of the piles exacerbates this stress redistribution, significantly impacting structural stability. In the surface layer of the landslide, stress at the frictional soil arch can plummet to as low as 50% of standard conditions, diminishing overall stability and heightening the risk of differential deformation between the piles and the surrounding soil.

The stability of a landslide pile is closely related to the integrity of the soil arch. Both end-bearing and frictional soil arches contribute significantly to the stability of the support system, with the former mainly transferring most of the landslide forces to the piles. However, variations in soil parameters and external disturbances, such as a drop in reservoir level, directly affect the bearing capacity of the soil arch. Frictional soil arches are particularly sensitive to these external disturbances. When soil slip occurs, the effectiveness of the friction-type soil arch effect is significantly reduced, jeopardising the slip resistance. This degradation results in a substantial decrease in pile stability, particularly when the frictional soil arch fails to function as intended. Therefore, to ensure the long-term stability of anti-slide pile systems in reservoir bank landslide management, it is crucial to continuously monitor and reinforce the integrity of the soil arch.

6 Conclusion

This study on the Shilongmen accumulation layer landslide yields the following conclusions.

(1) As the shear strength parameters of the soil decrease, the soil arching effect progressively weakens, leading to more uneven stress transmission across the sliding surface and increasing the risk of slip. The end-bearing soil arch demonstrates superior force transmission compared to the friction soil arch. Therefore, the variability of soil strength parameters should be fully considered during the design phase of anti-slide piles to optimize the soil arching effect, thereby enhancing the stability and anti-sliding capacity of the structure.

(2) As the sliding area expands, the stress on the soil in front of the piles gradually decreases, while the friction effect of the soil arch weakens, impacting the overall stability of the structure. The friction soil arch is more sensitive to soil slip in front of the pile, with lateral displacement along the pile side further reducing its effectiveness during the sliding process. Additionally, localized "bypass flow"

phenomena may occur between piles, adversely affecting the soil arching effect and compromising the structural integrity as a whole.

(3) Under landslide driving forces, deformation incompatibility occurs between the soil and the anti-slide piles, leading to pile-soil separation. Generally, the displacement of the friction soil arch between piles is greater than that of the end-bearing soil arch behind the piles. To address this issue, it is recommended to install barriers between the anti-slide piles to control soil deformation, thereby mitigating the negative effects of soil sliding in front of the piles. Additionally, it is suggested to install prestressed anchors at the rear edge of the anti-slide piles to enhance the overall stability of the anti-slide pile system.

Data availability statement

The raw data supporting the conclusions of this article will be made available by the authors, without undue reservation.

Author contributions

GL: Data curation, Methodology, Writing–original draft, Writing–review and editing. CZ: Funding acquisition, Investigation, Supervision, Validation, Visualization, Writing–original draft, Writing–review and editing, Resources. ZQ: Investigation, Writing–review and editing. HX: Writing–review and editing, Investigation.

Funding

The author(s) declare that financial support was received for the research, authorship, and/or publication of this article. National Natural Science Foundation of China (NSFC) Young Scientists Fund Project (41002112).

Acknowledgments

The authors express their heartfelt gratitude to their advisor for providing insightful guidance and constructive feedback throughout the course of this research. The advisor's expertise and encouragement have been invaluable in shaping the study. The authors also acknowledge the use of advanced computational tools and facilities, which significantly contributed to the analyses presented in this work. Special appreciation is extended to all those who assisted with data collection, technical support, and manuscript preparation. This research was generously supported by the National Fund Project, whose financial assistance was instrumental in enabling the study. Finally, the authors thank the reviewers for their thoughtful comments and suggestions, which have greatly improved the quality of this work.

Conflict of interest

The authors declare that the research was conducted in the absence of any commercial or financial relationships that could be construed as a potential conflict of interest.

Generative AI statement

The author(s) declare that no Generative AI was used in the creation of this manuscript.

Publisher's note

References

Chen, G., Zou, L., Wang, Q., and Zhang, G. (2020). Pile-Spacing calculation of Anti-Slide pile based on soil arching effect. *Adv. Civ. Eng.* 1, 1211–1216. doi:10.1155/2020/7149379

Fang, K., Tang, H., Li, C., Su, X., An, P., and Sun, S. (2023). Centrifuge modelling of landslides and landslide hazard mitigation: a review. *Geosci. Front.* 14, 101493. doi:10.1016/j.gsf.2022.101493

Fu, Y. (2017). *Analysis of anti slide pile arch development mechanismand parameter influence. MA thesis*. Chongqing Jiaotong University. Master's degree thesis.

Gao, P. (2023). Study on soil arching effect and landslide thrust of anti slide piles inreservoir bank landslides. *Master's thesis, Wuhan Inst. Technol.* doi:10.27727/d.cnki.gwhxc.2023.000233

Hu, X., Zhou, C., Xu, C., Liu, D., Wu, S., and Li, L. (2019). Model tests of the response of landslide-stabilizing piles to piles with different stiffness. *Landslides* 16, 2187–2200. doi:10.1007/s10346-019-01233-4

Huang, J., Zhao, J., Duan, X., and Zhang, J. (2020). Reliability analysis for soil slopes reinforced with piles using shear strength reduction method. *J. Civ. Environ. Eng.* 42, 11–18. doi:10.11835/j.issn.2096-6717.2020.062

Li, C., Criss, R. E., Fu, Z., Long, J., and Tan, Q. (2021). Evolution characteristics and displacement forecasting model of landslides with stair-step sliding surface along the Xiangxi River, three Gorges Reservoir region, China. *Eng. Geol.* 283, 105961. doi:10.1016/j.enggeo.2020.105961

Li, H., Ni, W., Li, G., and Wang, D. (2020). Determination of maximum pile spacing of anti-slide pile with rectangular section considering soil arching effects. *IOP Conf. Ser. Earth Environ. Sci.* 560, 012045. doi:10.1088/1755-1315/560/1/012045

Li, Z., and Huang, D. (2023). Stability analysis of a water-rich slope stabilized by a novel upper-hollow drainage anti-slide pile. *Nat. Hazards* 117, 425–446. doi:10.1007/s11069-023-05866-6

Liu, X., Cai, G., Liu, L., and Zhou, Z. (2020). Investigation of internal force of anti-slide pile on landslides considering the actual distribution of soil resistance acting on anti-slide piles. *Nat. Hazards* 102, 1369–1392. doi:10.1007/s11069-020-03971-4

Liu, Z., Yan, Z., Wang, X., Li, J., and Qiu, Z. (2021). Effect of the inclined pile-soil arch in a soil landslide reinforced with anti-sliding piles. *Nat. Hazards* 106, 2227–2249. doi:10.1007/s11069-021-04541-y

Peerun, M., Ong, D., Choo, C., and Cheng, W. (2020). Effect of interparticle behavior on the development of soil arching in soil-structure interaction. *Tunn. Undergr. Sp. Tech.* 106, 103610. doi:10.1016/j.tust.2020.103610

Ren, X., Luo, L., Zheng, Y., Ma, J., and An, X. (2022). Morphological evolution of passive soil arch in front of horizontal piles in three dimensions. *Buildings* 12, 1056. doi:10.3390/buildings12071056

Tang, H., Li, C., Gong, W., Zou, Z., Zhang, Y., Zhang, S., et al. (2022). Fundamental attribute and research approach of landslide evolution. *Earth Sci.* 47, 4596–4608. doi:10.3799/dqkx.2022.461

Wang, G., Hao, L., and Tian, Y. (2023). Study on the formation mechanism and risk prediction of high-level accumulation landslides in Bailongjiang River Basin, Gansu Province. *Chin. J. Rock Mech. Eng.* 42, 1003–1018. doi:10.13722/j.cnki.jrme.2022.0428

Wang, L., Jia, H., Jiang, T., Zhang, J., Jia, Y., Li, L., et al. (2024). Novel evaluation method based on critical arch height as instability criterion for sustaining arch locked-segment-type slopes. *Sci. Rep.* 14, 7991. doi:10.1038/s41598-024-58737-w

Xiang, J. (2019). *The response law of groundwater dynamics tofluctuation of reservoir water level in complex landslide structures and its application*. China University of Geosciences. Master's degree thesis.

Xu, C. (2020). *Study on slope stability and soil arch effect of anti slide pile based on FLAC3D. MA thesis*. Chang'an: University.

Xu, Y., Li, Y., Li, S., and Shi, H. (2024). Seepage-deformation mechanism of colluvial landslides under the action of reservoir water level decline and rainfall. *Bull. Geol. Sci. Technol.* 43 (1), 216–228. doi:10.19509/j.cnki.dzkq.tb20220417

Ye, G., Li, L., Zhen, Z., Feng, J., and Bin, N. (2022). Model tests on influences of fill density on soil arching effects using transparent soil. *Chin. J. Geotechnical Eng.* 44, 20–24. doi:10.11779/CJGE2022S2005

Yu, H., Li, C., Zhou, J., Gu, X., Duan, Y., Liao, L., et al. (2022). A large-scale obliquely inclined bedding rockslide triggered by heavy rainstorm on the 8th of July 2020 in Shiban Village, Guizhou, China. *Landslides* 19, 1119–1130. doi:10.1007/s10346-022-01850-6

Zeng, T., Yin, K., Gui, L., Peduto, D., Wu, L., Guo, Z., et al. (2023). Quantitative risk assessment of the shilongmen reservoir landslide in the three Gorges area of China. *Bull. Eng. Geol. Environ.* 82 (6), 214. doi:10.1007/s10064-023-03242-z

Zhang, C., Yin, Y., Yan, H., Zhu, S., Li, B., Hou, X., et al. (2023). Centrifuge modeling of multi-row stabilizing piles reinforced reservoir landslide with different row spacings. *Landslides* 20, 559–577. doi:10.1007/s10346-022-01994-5

Zhang, L., Zhu, H., Han, H., and Shi, B. (2024). Fiber optic monitoring of an anti-slide pile in a retrogressive landslide. *J. Rock Mech. Geotechnical Eng.* 16 (1), 333–343. doi:10.1016/j.jrmge.2023.02.011

Zhang, S., Li, C., Qi, H., Chen, X., and Ma, S. (2021). Soil arch evolution characteristics and parametric analysis of slope anchored anti-slide pile. *KSCE J. Civ. Eng.* 25, 4121–4132. doi:10.1007/s12205-021-1612-6

Zhang, Y. (2018). *Multi-field characteristics and evolution mechanism of majiagou landslide- stablizing piles system under reservoir operations*. China University of Geosciences. Master's degree thesis.

Zhong, W., Zhang, S., and He, N. (2022a). Experimental study on soil arch behind anti-slide pile based on relativedeformation method. *Rock Soil Mech.* 43, 315–326. doi:10.16285/j.rsm.2021.1028

Zhong, W., Zhang, S., and He, N. (2022b). An experimental study on the dynamic evolution characteristics of soil arching and the rational spacing of anti-slide piles. *Sustainability* 14, 8566. doi:10.3390/su14148566

Zhou, C., Shao, W., and van, W. (2014). Comparing two methods to estimate lateral force acting on stabilizing piles for a landslide in the Three Gorges Reservoir, China. *Eng. Geol.* 173, 41–53. doi:10.1016/j.enggeo.2014.02.004

Zhou, C., Shao, W., Yin, K., and Yang, Z. (2018). Estimating the properties of weathered bedrock and pilerock interaction from the geological strength index. *J. Mt. Sci.* 15, 1757–1776. doi:10.1007/s11629-017-4576-8

Zhou, C., Zhu, R., He, Q., and Sun, D. (2022). Study on the variation law of sliding soil strength under different dry-wet cycles. *J. Disaster Prev. Reduct.* 38, 1–8. doi:10.13693/j.cnki.cn21-1573.2022.02.001

Zhu, R. (2022). Study on strength characteristics and slope stability of sliding zonesoil of shilongmen landslide in wanzhou district of three Gorges reservoir area. *Master's thesis, Wuhan Inst. Technol.* doi:10.27727/d.cnki.gwhxc.2022.000439